RSC Advances

ROYAL SOCIETY OF CHEMISTRY

www.rsc.org/advances

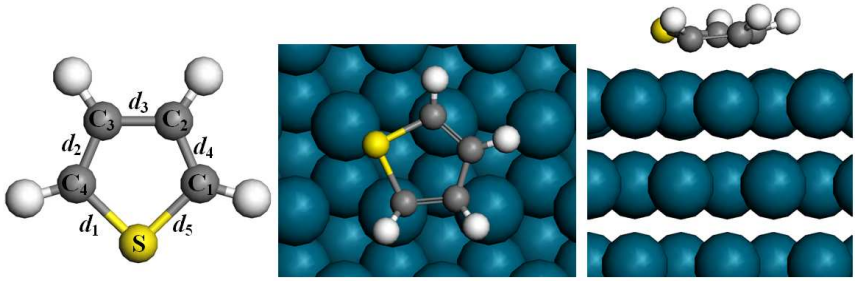

The parallel adsorption of thiophene molecule on Pd(111) surface at the hollow site through the ring plane is the most stable. The direct hydrodesulfurization mechanism had low activation energy, but the product has more than one possibility and is difficult to control. The mechanism of indirect hydrodesulfurization was best fit for the 1,2-cis-hydrogenation process. The most feasible reaction pathway are (1) $C_4H_4S+H_2 \rightarrow \alpha,\beta\text{-}C_4H_6S$; (2) $\alpha,\beta\text{-}C_4H_6S+H_2 \rightarrow C_4H_8S$; (3) $C_4H_8S+H_2 \rightarrow C_4H_{10}+S$.

DFT investigations of the adsorption and hydrodesulfurization mechanism of thiophene catalyzed by Pd(111) surface

Wei Shi, Lianyang Zhang, Zheming Ni*, Shengjie Xia, Xuechun Xiao

Laboratory of Advanced Catalytic Materials, College of Chemical Engineering and Materials Science, Zhejiang University of Technology, Hangzhou 310032, Zhejiang, China

* Corresponding author.

E–mail: jchx@zjut.edu.cn, nzm@zjut.edu.cn

Telephone number: 086–0571–88320373

Abstract:

The adsorption behavior and the selective hydrodesulfurization mechanism of thiophene on Pd(111) surface were elucidated by density functional theory (DFT). All the pertinent species of different pathways were gathered to obtain their preferred adsorption sites. The activation energy and reaction energy of each step in different pathways were also calculated. The results show that the adsorption at the hollow site was the most stable when the thiophene was in parallel to the Pd(111) surface with ring plane. In the process of hydrodesulfurization, the reaction heat was almost negative, therefore reducing the temperature is helpful to the removal of S atom. The direct hydrodesulfurization mechanism had low activation energy, but the product has more than one possibility and is difficult to control. The mechanism of indirect hydrodesulfurization was best fit for the 1,2-cis-hydrogenation process. The most feasible reaction pathway are (1) $C_4H_4S+H_2 \rightarrow \alpha,\beta\text{-}C_4H_6S$; (2) $\alpha,\beta\text{-}C_4H_6S+H_2 \rightarrow C_4H_8S$; (3) $C_4H_8S+H_2 \rightarrow C_4H_{10}+S$. Among different steps, the formation of C_4H_8S is the rate-determining step.

Key words: Density functional theory; Thiophene; Pd(111); Adsorption; Hydrodesulfurization mechanism

1. Introduction

Thiophene is a group of basic constituents contained in fuel oil and is considered to be one of the primary causes of acid rain to the environment[1-3]. With the increasing consumption of fossil based fuel oil, many stringent environmental

regulations have been applied in many countries to reduce the sulfur levels in fuel oil. As a result, the interest in the research of desulfuration of thiophene has increased dramatically[4-7].

At present, by comparison with the non-hydrodesulfurization (NHDS) method for sulfur removal, the method of hydrodesulfurization (HDS) is more mature, more effective and more economical[1,8,9]. Most previous studies focused on the application of precious metal catalysts in the HDS of thiophene, which has superior catalytic activity and milder reaction conditions[10,11]. Among these catalysts, palladium (Pd) nanoparticles is one of the most effective precious metal catalysts, which is characterized by high degree of dispersion and small average particle size[12,13], and it has been widely applied in the hydrogenation reactions of thiophene. Badano *et al.*[14] compared sulfur resistance of different catalysts, the result shows that the Pd catalyst had the highest activity. Vit *et al.*[15] synthesized Pd/silica-alumina and the result suggests that the higher acidity and surface area could improve the activities of Pd catalyst in HDS of thiophene. Besides, they also found that the PdH_x phase was most likely served as a storage medium during the hydrogenation reaction[16]. Although there were extensive experimental researches on the hydrogenation reaction of thiophene, only a few reported its adsorption process and hydrogenation mechanism, due to the complexity of experiment and the limitation of the characterization methods.

Density Functional Theory[17,18] has been widely used to calculate the adsorption energy, structure parameter, activation energy and reaction energy in the process of

different reactions. Liao *et al*.[19] made comparisons among different Mo-catalysts during the C-S cleavage of thiophene in order to find the most active catalyst species. Also by DFT, Zhu *et al*.[20,21] researched the hydrogenation reaction of thiophene over Pt(110) and Pt(111) surface to present the most efficient reaction route. Our previous work[22] predicted the most favorable mechanism of thiophene catalyzed on Au(111) surface, and found that the hydroisomerization process is dominant.

In this work, we studied the adsorption process and hydrogenation mechanism of thiophene on clean Pd(111) surface by DFT method using Dmol^3 program package. The properties of different adsorption sites were also elucidated, which include structure parameter and adsorption energy. Furthermore, the possible reaction pathways of thiophene hydrogenation were discussed in detail to discover the primary HDS mechanism. The aim of this work is to provide a better understanding of the structural, energetic, catalytic and selective properties of Pd catalysts for the hydrodesulfurization of thiophene.

2 Computational Details

2.1 Calculation methods

The density functional calculations shown in this work were done with the DMol^3[23] program package by using the Materials Studio 5.5 of Accelrys Inc. The exchange-correlation functional of Perdew and Wang (PW91)[24-26] is used to calculate the electronic structure with the generalized gradient approximation (GGA). The valence electron functions were expanded into a set of numerical atomic orbitals by a

double-numerical basis with polarization functions (DNP). The tolerances of energy, force and displacement convergence were 5×10^{-4} eV, 2×10^{-2} eV•nm^{-1} and 5×10^{-4} nm, respectively. The maximum self-consistent field (SCF) cycles were 1000 with a tolerance of 2×10^{-4} eV and the k-point was set to 1×1×1. The transition state (TS) structures were computed by using the Complete LST/QST tools[27] to investigate the minimum energy pathway for the hydrogenation of thiophene. In addition, each TS was verified by only one imaginary frequency. Throughout calculations, smearing was employed to accelerate convergence of orbital occupation with convergence value of 0.002 Ha and all of the computations were performed with spin-polarization.

2.2 Surface model

In order to make a good balance among the calculation accuracy, calculation efficiency and the complexity of thiophene molecular, we modeled the Pd(111) crystal surface to simulate the exposed Pd atoms. The periodical surface was modeled by three-layer slabs with a 4 × 4 unit cell which contains 48 Pd atoms to study the adsorption and the hydrogenation of the thiophene molecular systems, as shown in Figure 1. Only one thiophene molecule was adsorbed on one side of the slab, in other words, the coverage is 1/16 mono-layer (ML). The vacuum region thickness between the repeated slabs was 1 nm, which was large enough to avoid interactions between different slabs. The layer and the vacuum region could form a unit which was repeated periodically in the space. In the process of geometry optimization and TS search, the upmost two Pd layers were allowed to relax freely, and the bottom layer

was frozen. Under the computational conditions mentioned above, the lattice parameter of Pd(111) surface was calculated to be 0.3893 nm, which is in good agreement with the experimental value of 0.3895 nm[28,29]. These results show that the method of calculation in this paper is reliable.

(Insert Figure 1)

3. Results and Discussion

3.1. Adsorption Energies and Geometries Analysis

Calculations of the adsorption energies of thiophene on Pd(111) surfaces were performed in order to discuss the HDS mechanisms of thiophene on Pd substrates during the initial stage. In the present work, the adsorption energies (E_{ads}) is calculated using the equation below:

$$E_{ads} = E_{(A/surface)} - (E_A + E_{surface})$$

where $E_{(A/surface)}$ is the total energy of the Pd(111) surface with thiophene molecule onto it, $E_{surface}$ is the energy of the Pd(111) surface without the thiophene molecule and E_A is the energy of free thiophene molecule. With this definition, E_{ads} generally has a negative value, and a larger value which corresponds to more stable adsorption on Pd(111) surface.

According to the previous works[22,30], the thiophene plane would interact with metal surface through the S atom. In addition, the vertical adsorption sites would be converted to parallel adsorption sites, this implies that the model of parallel

adsorption is more stable. As a result, we chose twelve highly symmetric parallel adsorption sites on the Pd(111) surface for calculations, as shown in Fig. 1. These adsorption sites include top(0°、30°、60°), hcp(0°、30°、60°), fcc(0°、30°、60°) and bridge(0°、30°、60°) sites. As can be seen in the Fig. 1, The 0°, 30° and 60° represent the adsorption sites with the symmetry axis rotating 0°, 30° and 60° from the horizontal direction.

(Insert Table 1)

The adsorption energies and geometric parameters of different sites were calculated and listed in Table 1, only those in stable adsorption configurations were summarized. Besides, the most stable structure of thiophene adsorbed on Pd(111) surface is shown in Fig. 2. As seen from Table 1 and Fig. 2, thiophene molecule adsorbed on Pd(111) surface with the energy of -176 to -186 kJ•mol^{-1}, and preferred to adsorbed in a parallel way through the ring plane. Among different initial adsorption sites, the E_{ads} of Bri-0° site is -185.3 kJ•mol^{-1} and the distance between Pd atom and S atom is 0.1461 nm. The maximum of E_{ads} and the least value of $d_{Pd\text{-}S}$ suggest that the position of Bri-0° is the most stable. During the process of adsorption, the S atom and H atoms of thiophene move upward and the axial rotation of the ring plane is clockwise. Finally, the S atom of thiophene transferred to the hollow site and interacted with Pd(111) surface.

(Insert Figure 2)

In order to analyze the structure parameter of the most stable adsorption site of thiophene molecule on Pd(111) surface, Table 2 lists the adsorption energy and bond lengths of thiophene molecule at the initial site of Bri-0°. By comparing the data in Table 2, it can be seen that the calculation of bond length for free thiophene is in good agreement with the experimental values[30]. After adsorption, there is an elongation in the range of 0.0013-0.0112 nm for the bond length of d_1-d_5, while the energy of thiophene decreased. This phenomena suggests that the adsorption of thiophene on Pd(111) surface could promote the hydrogenation reaction. In addition, the greatest change in d_1 implies that the H atom is more likely to attack the α-C of thiophene.

(Insert Table 2)

3.2. Hydrogenation mechanism of thiophene

Based on the previous studies[21,31-35], it is already known that there exist two different competing reaction pathways, as can be seen in Fig. 3. The first one is termed the direct desulfurization (DDS) pathway, which would generate S atom and butadiene without further hydrogenation. In contrast, the second one is termed the hydrogenation (HYD) pathway and the major product are S atom and n-butane.

(Insert Figure 3)

(Insert Table 3)

Table 3 provides six possible hydrogenation mechanisms of thiophene on Pd(111) surface. The mechanisms of A-E represent the HYD pathway and the mechanisms of F represents the DDS pathway. Among hydrogenation mechanism of A-F, the major difference is the diversity of hydrogenation position of α-C and β-C in thiophene molecule. According to the mechanisms of A-F in Table 3, we optimized the structures of reactants (IS) and products (FS), and then searched TS between them. The activation energies and reaction energies at TS are tabulated in Table 4. Among different hydrogenation mechanisms, the initial step is the coadsorption of thiophene and atomic H, so we only compared the intermediate steps of hydrogenation process in Table 3 (Step1-Step4).

(Insert Table 4)

3.2.1 HYD mechanism of thiophene

At the outset of the HYD reaction, we considered two possible active sites in thiophene molecule, including α-C and β-C. The calculated barriers (*Ea*), the total energy change (ΔE), and the corresponding TS structures for the mechanism of A-E(1) are shown in Fig. 4.

$C_4H_4S^*+H^* \rightarrow C_4H_5S^*$ (FS1 or FS2)

For the reaction of $C_4H_4S^*+H^* \rightarrow \alpha$-$C_4H_5S^*$(FS1), we calculated the coadsorption of thiophene and atomic H as IS1. After complete optimization, thiophene adsorbed with S atom downwardly bonding to the Pd(111) surface at the original hollow site, meanwhile, the C_2 and C_3 atoms of thiophene moved upward. The atomic H transferred from the fcc site to the neighboring bridge site. In the TS1, the reacted α-C tilted by 38.4° from the horizontal plane and the atomic H moved to the hcp site with α-C-H distance of 0.1756 nm. Once FS1 was formed, the reacted H of α-C continued tilting upward to perpendicular to the Pd(111) surface. Finally, the FS1 adsorbed at hollow site through the unreacted double bond of C=C to the surface. The bond length of the reacted α-C-H decreased from 0.2729 nm to 0.1095 nm and the d_1 was elongated to 0.1841 nm. This reaction was exothermic by -54.6 kJ•mol^{-1} and the corresponding *Ea* was 41.6 kJ•mol^{-1}.

For the reaction of $C_4H_4S^*+H^* \rightarrow \beta$-$C_4H_5S^*$(FS2), the IS of the first step is exactly the same as the IS1. In TS2, the S atom tilted upward slightly and the atomic H moved gradually far away from the surface at the same time. The bond length of the reacted β-C-H decreased from 0.2366 nm in the IS1 to 0.1597 nm. As long as FS2 was formed, the reacted H of β-C kept tilting upward to perpendicular to the Pd(111) surface, meanwhile, the S atom moved upward obviously. This reaction was exothermic by -50.7 kJ•mol^{-1} and the corresponding *Ea* was 85.6 kJ•mol^{-1}.

(Insert Figure 4)

As can be seen from Table 4 and Figure 4, the relative energy of FS1 and FS2 is exothermic with negative value, which indicates that reducing the temperature is helpful for the reaction of step 1. In addition, the formation of FS1 is more favorable because of the comparably lower activation energy of 41.6 kJ•mol^{-1}. Therefore, the hydrogenation process of α-C in thiophene is easier to occur in step 1, and this result is in good agreement with the analysis of the structure parameters in section 3.1.

α-C_4H_5S*+H *→C_4H_6S* (FS3 or FS4)

α-C_4H_5S* is regarded as the dominant product in step 1, and the further hydrogenation process would occur on the basis of α-C_4H_5S*. The *Ea*, ΔE and the corresponding TS structures for the mechanism of A-C(2) are shown in Fig. 5.

For the reaction of α-C_4H_5S*+H *→α,β-C_4H_6S*(FS3), we calculated the coadsorption of α-C_4H_5S and atomic H as IS2. When the reaction happened, the methylene of α-C_4H_5S tilted upward and other C atoms lie flush with each other. The atomic H transferred from the fcc site to the neighboring hcp site. In TS3, the reacted β-C-H moved upward and the atomic H got close to the ring plane. The product α,β-C_4H_5S* (FS3) was generated after the atomic H catching the reacted β-C and sat at the hollow site through the double bond. The d_1 was elongated to 0.1852 nm. This reaction was exothermic by -22.9 kJ•mol^{-1} and the corresponding *E*a was 142.1 kJ•mol^{-1}.

For the reaction of α-C_4H_5S*+H *→α,α-C_4H_6S*(FS4), the reactant of it is the

same as the IS2. In TS4, the reacted α-C moved upward and the atomic H transferred to the adjacent hcp site in order to get close to the reacted α-C with the α-C-H distance of 0.2200 nm. Besides, the atoms of C_2 and C_3 are electron-rich because of the hydrogenation process of α-C, as a result, the double bond between C_2 and C_3 was formed during the reaction. Once FS4 was produced, the H atoms of α-C kept almost the same structure, both of which had a tilting angle of 109.5°. Finally, the FS4 adsorbed at bridge site via the double bond of C_2 and C_3. This reaction was endothermic by 21.3 kJ•mol^{-1} and the corresponding *E*a was 185.6 kJ•mol^{-1}.

(Insert Figure 5)

Compared with the calculation results in step 2, the formation of α,β-C_4H_5S* is exothermic, while the formation of α,α-C_4H_5S* is endothermic. The hydrogenation process of C_4H_5S* to α,β-C_4H_5S* seems more likely to take place due to its lower energy barrier (142.1 kJ•mol^{-1}). Below, the α,β-C_4H_5S* species is hence selected as the species for the further hydrogenation.

α, β-C_4H_6S*+H*→C_4H_7S* (FS5 or FS6)

α, β-C_4H_6S* is considered as the most favorable product in step 2, and the further hydrogenation process of α,β-C_4H_6S leads to α,β,α-C_4H_6S or α,β,β-C_4H_6S. The *Ea*, ΔE and the corresponding TS structures for the mechanism of A-B(3) are illustrated in Fig. 6.

The reaction of α,β-C_4H_6S*+H*→α,β,α-C_4H_7S*(FS5) starts from the coadsorption of α,β-C_4H_6S and atomic H. In the initial state, the structure of α,β-C_4H_6S remained the same as the FS3, and located at hollow site through the double bond. The atomic H transferred to the adjacent hcp site. In TS5, the atomic H left its hcp site and moved to the adjacent hcp site and the ring plane rotated anticlockwise to meet with the attacking H atom. The forming α-C-H distance decreased from 0.3582 nm to 0.2531 nm. Once FS5 was formed, the S atom moved away from Pd surface and the ring plane tilted downwards. The bond length of the reacted α-C-H decreased to 0.1225 nm. This reaction was endothermic by 85.3 kJ•mol^{-1} and the corresponding *Ea* was 124.2 kJ•mol^{-1}.

For the reaction of α,β-C_4H_6S*+H*→α,β,β-C_4H_7S*(FS6), the reactant of it was the same with what was described in IS3. In TS6, the atomic H transferred from the hcp site to the neighboring top site. At the same time, the atoms of C_2 and C_3 moved upwards. The distance between the atomic H and reacted β-C was decreased to 0.2128 nm from 0.2929 nm. As long as FS6 was produced, the C_2 and C_3 further moved upward. Subsequently, the β-C-H bond was activated with the distance of 0.1102 nm and the d_1 was elongated to 0.1860 nm. This reaction was exothermic by -36.6 kJ•mol^{-1} and the corresponding *Ea* was 110.1 kJ•mol^{-1}.

(Insert Figure 6)

As can be seen from the data above, the reactant of α,β-C_4H_6S prefers

hydrogenation on β-C rather than α-C. The formation of FS5 is endothermic, while the formation of FS6 is exothermic. Furthermore, a low barrier of 110.1 kJ•mol^{-1} as well as a short bond length of 0.1102 nm are present for the β-C-H bond formed in FS6. Therefore, the formation of FS6 from α,β-C_4H_6S is likely to occur.

α,β,β-$C_4H_7S^*+H^*\rightarrow C_4H_8S^*$ (FS7)

From previous discussion, the mechanism B is regarded as the most favorable pathway. There is only one possibility for the further hydrogenation of α,β,β-C_4H_6S to form the saturate production of C_4H_8S. The *E*a, ΔE, and the corresponding TS structures for the mechanism of B(4) are illustrated in Fig. 7.

The reaction of α,β,β-$C_4H_7S^*+H^*\rightarrow\alpha,\beta,\beta,\alpha$-$C_4H_8S^*$(FS7) began with the coadsorption of α,β,β-C_4H_7S and atomic H, as can be seen in IS4. For IS4 adsorption on Pd surface, the preferential adsorption site was where the atomic H transferred to the nearby hcp site, and the α,β,β-C_4H_7S molecule was bind at hollow site via the S atom, where the adsorption configuration is the same as the FS6. In TS7, the unsaturated α-C moved upward and the atomic H transferred to the adjacent hollow site in order to form the saturated bond of α-C-H. The distance between the atomic H and unsaturated α-C decreased from 0.3466 to 0.2011 nm. Once FS7 adsorbed at top site through the S atom, C atoms of ring plane lie flush with each other in parallel to the Pd surface. The d_1 was elongated to 0.1866 nm. This reaction was exothermic by 11.3 kJ•mol^{-1} and the corresponding *Ea* was 229.9 kJ•mol^{-1}.

(Insert Figure 7)

$C_4H_8S^*+2H^*\rightarrow C_4H_{10}^*+S^*$ (FS8 and FS9)

In the final step, $C_4H_8S^*$ is further hydrogenated to n-butane and S atom by the help of atomic H. The *E*a, ΔE and the corresponding TS structures for the mechanism of B(5-6) are illustrated in Fig. 8.

The reaction of $C_4H_8S^*+H^*\rightarrow C_4H_9S^*$(FS8) was exothermic by -37.8 kJ•mol^{-1}, with the corresponding *Ea* of 198.8 kJ•mol^{-1}. In the initial state, the molecule of C_4H_8S bound at top site through the S atom and the atomic H transferred from fcc site to the adjacent bridge site. In TS8, the atomic H moved close to the reacted α-C, resulting in a shortening of the distance between the α-C and atomic H from 0.3020 nm to 0.2257 nm. Besides, one of C-S bond broke up and the S atom moved downward to the Pd surface. The formed FS8 adsorbed at hcp site via S atom and the d_5 was elongated to 0.1879 nm, meanwhile, the distance between the α-C and the atomic H further reduced to the 0.1110 nm to form the bond of α-C-H.

For the reaction of $C_4H_9S^*+H^*\rightarrow C_4H_{10}^*+S^*$(FS9), we calculated the coadsorption of C_4H_9S and atomic H as IS6. After adsorption, the atomic H located at the original fcc site. The C_3 and C_4 atoms of C_4H_9S tilted upwards as compared with the structure in FS8. From the TS9 shown in Fig. 8, the atomic H located at the nearby top site, with α-C-H distance of 0.3756 nm, meanwhile, the S atom was separated from C_4H_9S. Once FS9 was produced, the dissociated S sat at fcc site and the molecule of C_4H_{10} adsorbed on Pd surface through the H atoms of C_2 and C_4, whose

structure was perpendicular to the Pd surface. These phenomenon is similar to the previous results reported in the literature[36]. This reaction was exothermic by -48.3 kJ•mol^{-1} and the corresponding *Ea* was 169.1 kJ•mol^{-1}.

(Insert Figure 8)

3.2.2 DDS mechanism of thiophene

Regarding DDS reaction, thiophene molecule would react with the atomic H, and then decompose into dissociated S and butadiene. The *Ea*, *ΔE* and the corresponding TS structures for the mechanism of F(1) and F(2) are shown in Fig. 9 and Fig. 10.

$C_4H_4S^*+H^* \rightarrow C_4H_5S^*$ (FS10)

For the reaction of $C_4H_4S^*+H^* \rightarrow C_4H_5S^*$(FS10), the configuration of reactant is the same as described in IS1. In TS10, d_5 decreased from 0.1820 nm to 0.1805 nm. This phenomena caused bond of d_1 to break, which was accompanied by migration of the atomic H to top site and upward migration of C_3 and C_4, respectively. As long as FS10 was formed, C_3 atom moved downward, which made the C_1-C_3 atoms parallel to Pd surface. Finally, FS10 adsorbed at hollow site on Pd surface via double bond of C_1 and C_2. This reaction was exothermic by -54.6 kJ•mol^{-1} and the corresponding *Ea* was 62.5 kJ•mol^{-1}.

(Insert Figure 9)

$C_4H_5S^*+H^* \rightarrow C_4H_6^*+S^*$ (FS11)

The reaction of $C_4H_5S^*+H^* \rightarrow C_4H_6S^*$(FS11) started from the coadsorption of C_4H_4S and atomic H. During the process, the atomic H migrated to hcp site from the initial fcc site and the structure of C_4H_5S remained the same as the FS10. Meanwhile, the bond of d_5 was elongated to 0.1843 nm. In TS11, the atomic H moved to the adjacent fcc site to form the bond of α-C-H, leading to the breaking of C-S bond. Then, the dissociated S transferred to hcp site. Once FS11 was produced, the dissociated S located at hcp site and the molecule of butadiene parallel adsorbed at bridge sites on Pd surface through the double bond of C_1=C_2 and C_3=C_4. This reaction was exothermic by -90.1 kJ•mol^{-1} and the corresponding *Ea* was 58.6 kJ•mol^{-1}.

(Insert Figure 10)

3.3 Brief summary about hydrogenation process of thiophene

We have investigated the overall reactions involving HYD and DDS mechanism of thiophene. On the basis of the discussed activation energies and reaction energies, the detailed potential energy diagram about HYD and DDS of thiophene on Pd(111) surface is shown in Fig. 11. As displayed in Fig. 11, the mechanism of DDS has a low energy of activation, but the product of butadiene would continue hydrogenating to produce monoolefine, alkane and so on. It is indicated that the product of DDS has more than one possibility and is difficult to control. For HYD mechanism, it is found

that the 1,2-cis-hydrogenation is dominant and the most favourable route for thiophene hydrogenation on Pd(111) surface is described as follows: $C_4H_4S \rightarrow \alpha\text{-}C_4H_6S \rightarrow \alpha,\beta\text{-}C_4H_6S \rightarrow \alpha,\beta,\beta\text{-}C_4H_6S \rightarrow C_4H_8S \rightarrow C_4H_9S \rightarrow C_4H_{10}+S$. This result are in good agreement with the experimental research[37]. During the process, the formation of C_4H_8S from $\alpha,\beta,\beta\text{-}C_4H_7S$ hydrogenation is considered as the rate-limiting step, whose energy barrier is the highest.

(Insert Figure 11)

4. Conclusion

In this paper, we have examined the adsorption process and hydrogenation mechanism of thiophene on Pd(111) surface in detail by performing periodic DFT calculations. Various adsorption modes of the intermediates involved in the reaction were investigated from the energetic and geometrical viewpoints, and the hydrogenation mechanism has been clarified.

Our results show that the parallel adsorption of thiophene at the hollow site through the ring plane is the most stable adsorption structure on Pd(111) surface. After thiophene adsorbs, all the bond length increase and the H atom is mostly like to attack the α-C of thiophene when the hydrogenation reaction occurs.

No matter what kind of mechanisms it is, the hydrogenation of thiophene is almost exothermic, so that reducing the temperature is beneficial to the desulfuration. For the DDS mechanism, the reaction has a lower energy of activation as compared

with HDS reaction, but the hydrogenated product has more than one possibility and is difficult to control. For HDS mechanism, it is found that the 1,2-cis-hydrogenation is predominate. During the reaction, the bond length of C-S in thiophene increases gradually while the bond energy of C-S decreases. All of these changes are helpful to the cleavage of C-S. The reaction path of HYD is found to proceed as follows: C_4H_4S → α-C_4H_6S → α,β-C_4H_6S → α,β,β-C_4H_6S → C_4H_8S → C_4H_9S → C_4H_{10}+S. The formation of C_4H_8S is considered as the rate-limiting step, whose energy barrier is the highest.

References

[1] S. Burnet, D. Mey, G. Perot, C. Bouchy and F. Diehl, *Appl. Catal. A-Gen*., 2012, **278**, 143-172.

[2] T. Ohshiro and Y. Izumi, *Biosci. Biotech. Bioch*., 1999, **63**, 1-9.

[3] B. Liu, Y. M. Chai, Y. P. Li, A. J. Wang, Y. Q. Liu and C. G. Liu, *Fuel*., 2014, **123**, 43-51.

[4] V. La Parola, M. L. Testa and A. M. Venezia, *Appl. Catal. B-Environ*., 2012, **119**, 248-255.

[5] L. M. Baldyga, S. O. Blavo, C. H. Kuo, C. K. Tsung and J. N. Kuhn, *ACS. Catal*., 2012, **2**, 2626-2629.

[6] V. La Parola, M. Kantcheva, M. Milanova and A. M. Venezia, *J. Catal*., 2013, **298**, 170-178.

[7] P. A. Nikulshin, V. A. Salnikov, A. V. Mozhaev, P. P. Minaev, V. M. Kogan and A.

A. Pimerzin, *J. Catal*., 2014, **309**, 386-396.

[8] H. Shang, W. Du, Z. C. Liu and H. C. Zhang, *J. Ind. Eng. Chem*., 2013, **19**, 1061-1068.

[9] A. Aguirre-Gutierrez, J. A. M. de la Fuente, J. A. de los Reyes, P. del. Angel and A. Vargas, *J. Mol. Catal. A-Chem*., 2011, **346**, 12-19.

[10] Z. J. Wu, S. Goel, M. Choi and E. Iglesia, *J. Catal*., 2014, **311**, 458-468.

[11] V. Gutierrez, F. Nador, G. Radivoy and M. A. Volpe, *Appl. Catal. A-Gen*., 2013, **464**, 109-115.

[12] F. A. Harraz, S. E. El-Hout, H. M. Killa and I. A. Ibrahim, *J. Mol. Catal. A-Chem*., 2013, **370**, 182-188.

[13] M. S. Lde, B. Hao, M. Neurock and R. J. Davis, *ACS. Catal*., 2012, **2**, 671-683.

[14] J. M. Badano, M. Quiroga, C. Betti, C. Vera, S. Canavese and F. Coloma-Pascual, *Catal. Lett*., 2010, **137**, 35-44.

[15] Z. Vit, H. Kmentova, L. Kaluza, D. Gulkova and M. Boaro, *Appl. Catal. B-Environ*., 2011, **108-109**, 152-160.

[16] Z. Vit, D. Gulkova, L. Kaluza and M. Boaro, *Appl. Catal. B-Environ*., 2014, **146**, 213-220.

[17] D. W. Heermann, *Computer Simulation Methods in Theoretical Physics*, Springer-Verlag, 1990.

[18] A. R. Leach, *Molecular Modelling: Principles and Applications*, Addison Wesley Longman Limitted Press, 2001.

[19] C. N. Liao, J. Y. Wang and B. Li, *J. Organomet. Chem*., 2014, **749**, 275-286.

[20] H. Y. Zhu, X. Q. Lu, W. Y. Guo, L. F. Li, L. M. Zhao and H. H. Shan, *J. Mol. Catal. A-Chem*., 2012, **363-364**, 18-25.

[21] H. Y. Zhu, W. Y. Guo, M. Li, L. M. Zhao, S. R. Li, Y. Li, X. Q. Lu and H. H. Shan, *Acs. Catal*., 2011, **11**, 1498–1510.

[22] Z. M. Ni, W. Shi, M. Y. Xia and J. L. Xue, *Chem. J. Chinese. Universities*., 2013, **34**, 2353-2362.

[23] B. Delley, *J. Chem. Phys*., 2000, **113**, 7756-7764.

[24] J. P. Perdew, J. A. Chevary, S. H. Vosko, K. A. Jackson, M. R. Pederson, D. J. Singh and C. Fiolhais, *Phys. Rev. B*., 1992, **46**, 6671-6687.

[25] J. A. White, D. M. Bird, M. C. Payne and I. Stich, *Phys. Rev. Lett*., 1994, **73**, 1404-1407.

[26] J. P. Perdew and Y. Wang, *Phys. Rev. B*., 1992, **45**, 13244-13249.

[27] T. A. Halgren and W. N. Lipscomb, *Chem. Phys. Lett*., 1977, **49**, 225.

[28] C. Kittel C, *Solid State Physics*, John Wiley & Sons, 1976.

[29] S. W. Mai, G. D. Zhou and W. J. Li, *Advanced inorganic structural chemistry*, Peking University Press, 2001.

[30] Z. H. Chen, K. N. Ding, X. L. Xu and J. Q. Li, *Chinese J. Struct. Chem*., 2010, **29**, 365-376.

[31] H. M. Wang and E. Iglesia, *Chemcatchem*., 2011, **3**, 1166-1175.

[32] R. Shafi and G. J. Hutchings, *Catal. Today*., 2000, **59**, 423-442.

[33] F. Besenbacher, M. Brorson, B. S. Clausen, S. Helveg, B. Hinnemann, J. Kibsgaard, J. V. Lauritsen, P. G. Moses, J.K. Nørskov and H. Topsøe, *Catal. Today*.,

2008, **130**, 86-96.

[34] L. Z. Dong, S. B. Duckett, K. F. Ohman and W. D. Jones, *J. Am. Chem. Soc*., 1992, **14**, 151-160.

[35] C. W. Benjamin and M. F. Cynthia, *Chem. Rev*., 1992, **92**, 491-504.

[36] M. L. Yang, Y. A. Zhu, C. Fan, Z. J. Sui, D. Chen and X. G. Zhou, *J. Mol. Catal. A-Chem*., 2010, **321**, 42-49.

[37] A. M. Veneziaa, R. Murania, V. L. Parola, B. Pawelec, J. L. G. Fierro, *Appl. Catal. A-Gen*., 2010, **383**, 211-216.

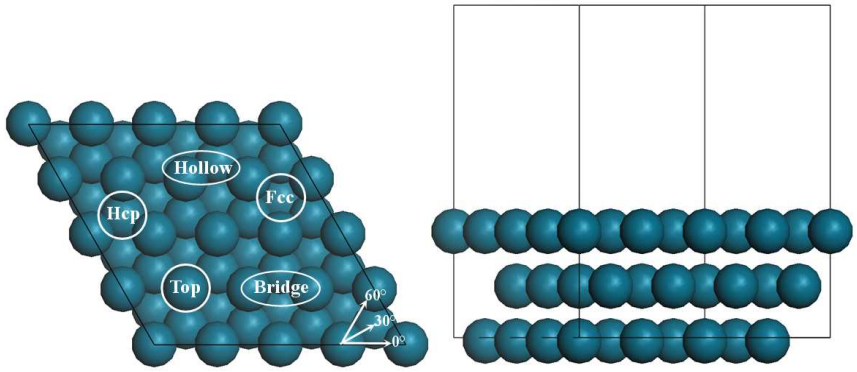

Fig. 1. The top(left) and side(right) view of Pd(111) surface models (4×4)

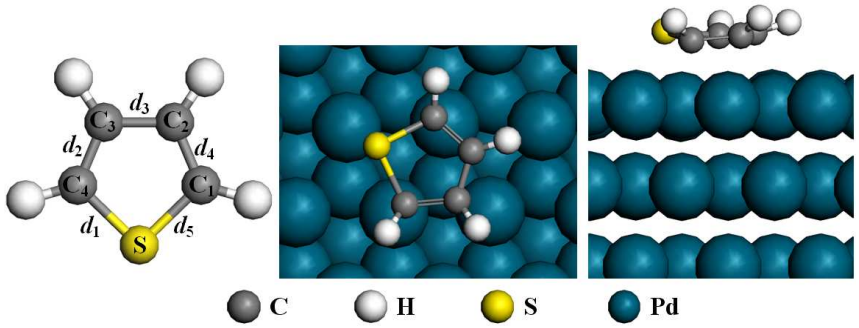

Fig. 2. The most stable configurations of thiophene on Pd(111) surface

(A) represented thiophene; (B) represented top view; (C) represented side view

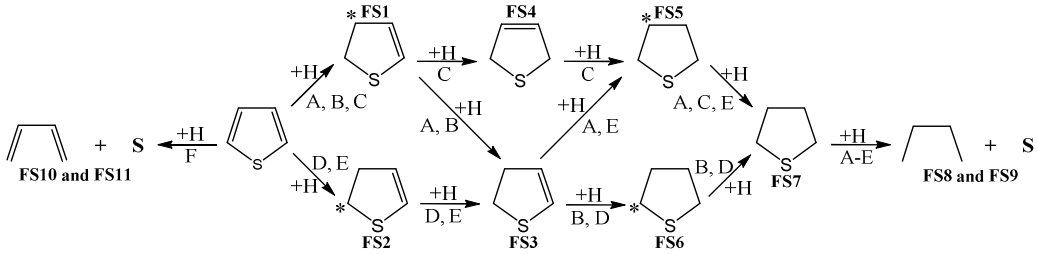

Fig. 3. Different reaction pathways for the hydrogenation of thiophene

A, B, C, D, E, F represents mechanism A, B, C, D, E, F

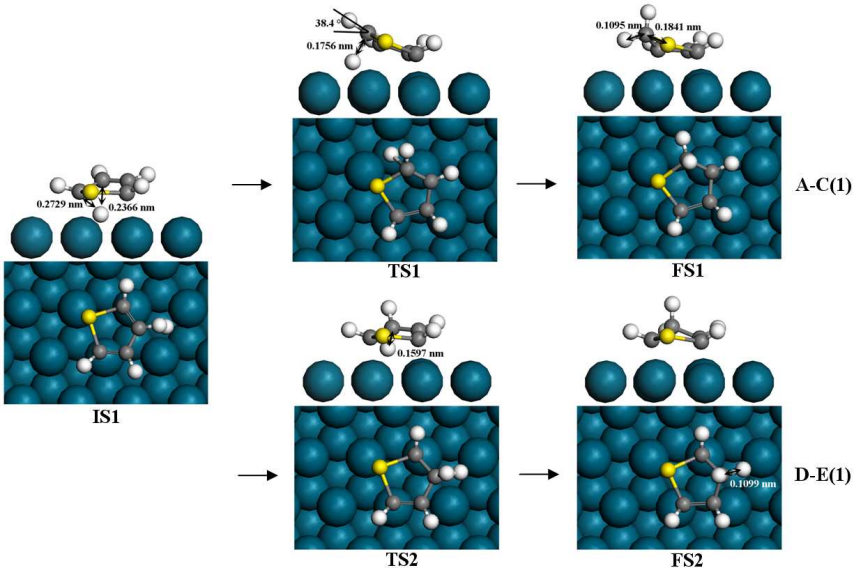

Fig. 4. The IS, TS, FS, activation energy and reaction energy (kJ•mol^{-1}) of mechanisms A-E(1) on Pd(111) surface

A-C(1): *Ea*=41.6; *ΔE*=-54.6 D-E(1): *Ea*=85.6; *ΔE*=-50.7

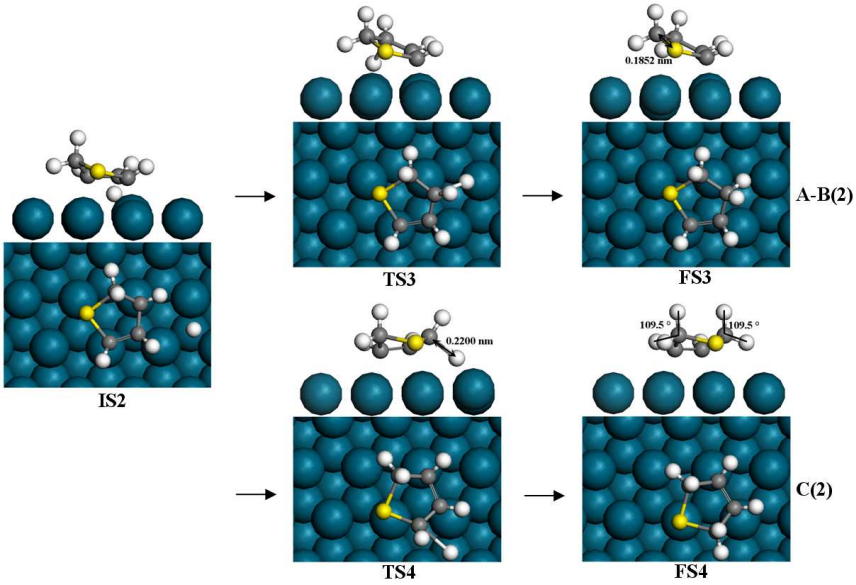

Fig. 5. The IS, TS, FS, activation energy and reaction energy (kJ•mol^{-1}) of mechanisms A-C(2) on Pd(111) surface

A-B(2): *Ea*=142.1; *ΔE*=-22.9 C(2): *Ea*= 185.6; *ΔE*=21.3

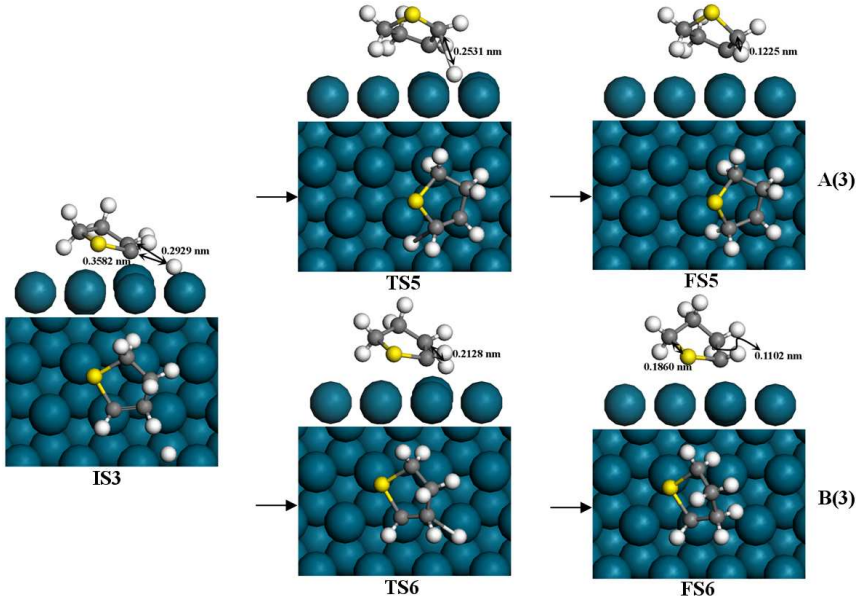

Fig. 6. The IS, TS, FS, activation energy and reaction energy(kJ•mol^{-1}) of mechanisms A-B(3) on Pd(111) surface

A(3): *Ea*=124.2; *ΔE*=85.3 B(3): *Ea*=110.1; *ΔE*=-36.6

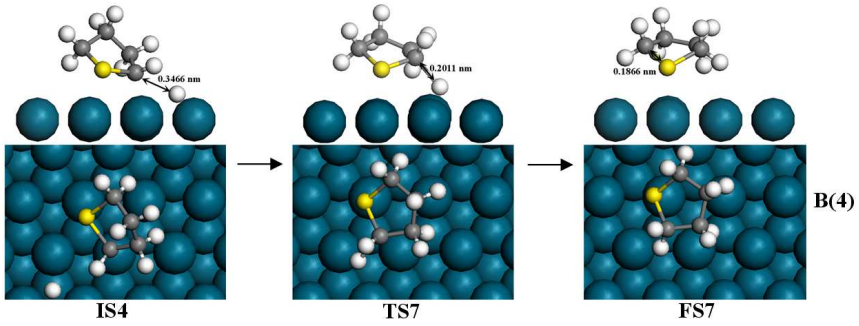

Fig. 7. The IS, TS, FS, activation energy and reaction energy (kJ•mol^{-1}) of mechanisms B(4) on Pd(111) surface

B(4): *Ea*=229.9; *ΔE*=11.3

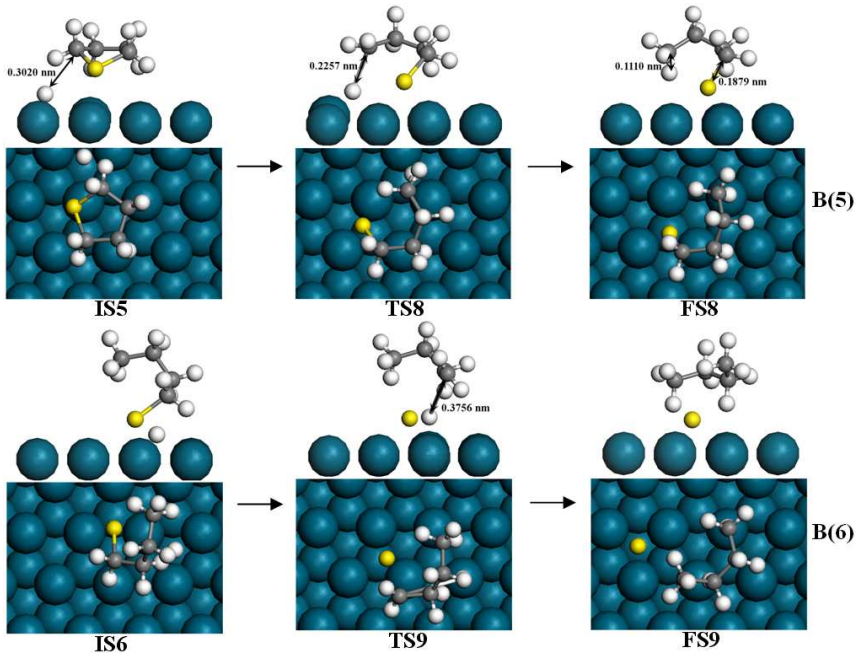

Fig. 8. The IS, TS, FS, activation energy and reaction energy (kJ•mol^{-1}) of mechanisms B(5-6) on Pd(111) surface

B(5): *Ea*=198.8; *ΔE*=-37.8 B(6): *Ea*=169.1; *ΔE*=-48.3

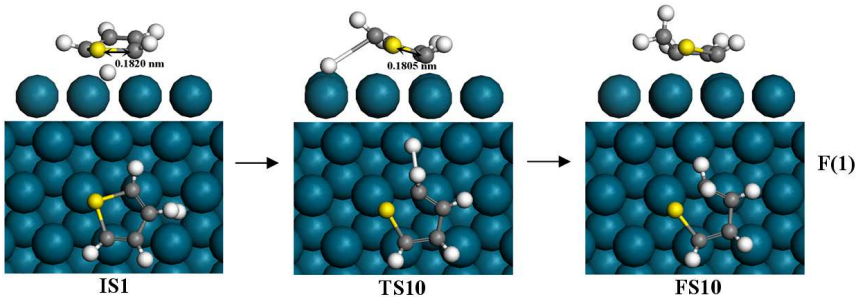

Fig. 9. The IS, TS, FS, activation energy and reaction energy (kJ•mol^{-1}) of mechanisms F(1) on Pd(111) surface

F(1): *Ea*=62.5; *ΔE*=-54.6

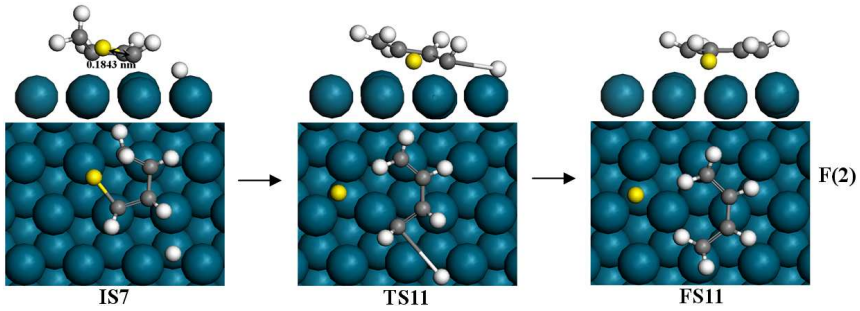

Fig. 10. The IS, TS, FS, activation energy and reaction energy (kJ•mol^{-1}) of mechanisms F(2) on Pd(111) surface

F(2): *Ea*=58.6; *ΔE*=-90.1

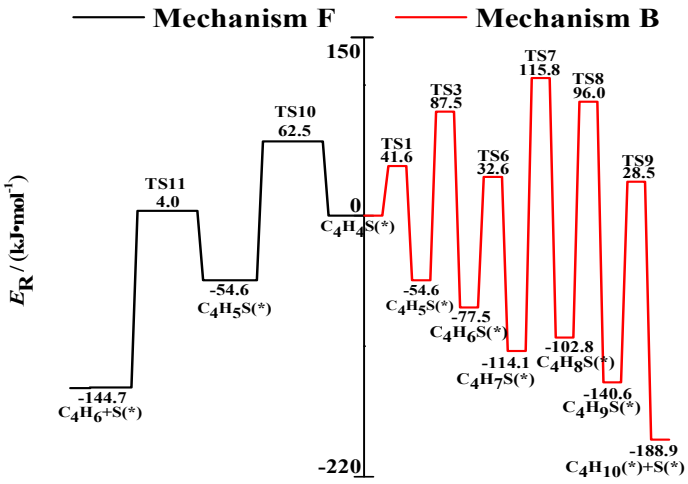

Fig. 11. Sketch for potential relative energy (E_R) of reaction mechanisms F and mechanisms B on Pd(111) surface

Table 1

Adsorption energies and geometric parameters of thiophene molecule on Pd(111) surface

Adsorption site	E_{ads}/(kJ•mol^{-1})	$d_{Pd\text{-}S}$/nm	Adsorption site	E_{ads}/(kJ•mol^{-1})	$d_{Pd\text{-}S}$/nm
Top-0°	-176.0	0.1559	Fcc-0°	-182.4	0.1578
Top-30°	-184.6	0.1587	Fcc-30°	-179.8	0.1516
Top-60°	-176.8	0.1560	Fcc-60°	-183.2-	0.1562
Hcp-0°	-181.6	0.1542	Bri-0°	-185.3	0.1461
Hcp-30°	-184.7	0.1584	Bri-30°	-184.5	0.1577
Hcp-60°	-182.1	0.1558	Bri-60°	-184.7	0.1551

The adsorption positions in table 1 represent the initial adsorption sites of thiophene

Table 2

Adsorption energy and bond lengths of thiophene molecule on Pd(111) for the most stable adsorption geometry

Model	E_{ads}/(kJ•mol^{-1})	d_1/nm	d_2/nm	d_3/nm	d_4/nm	d_5/nm
Thiophene (Expt)	—	0.1730	0.1370	0.1420	0.1370	0.1730
Thiophene (Calc)	—	0.1729	0.1372	0.1422	0.1372	0.1727
Thiophene / Au(111)	-185.3	0.1841	0.1424	0.1435	0.1482	0.1801
$\lvert\Delta d\rvert$	—	0.0112	0.0052	0.0013	0.0110	0.0074

Table 3

Reaction mechanisms of A-F for the hydrogenation of thiophene on Pd(111) surface

Step	Mechanism A	Mechanism B	Mechanism C
1	$C_4H_4S^*+H^*\rightarrow\alpha\text{-}C_4H_5S^*+*$		
2	$\alpha\text{-}C_4H_5S^*+H^*\rightarrow\alpha,\beta\text{-}C_4H_6S^*+*$		$\alpha\text{-}C_4H_5S^*+H^*\rightarrow\alpha,\alpha\text{-}C_4H_6S^*+*$
3	$\alpha,\beta\text{-}C_4H_6S^*+H^*\rightarrow\alpha,\beta,\alpha\text{-}C_4H_7S^*+*$	$\alpha,\beta\text{-}C_4H_6S^*+H^*\rightarrow\alpha,\beta,\beta\text{-}C_4H_7S^*+*$	$\alpha,\alpha\text{-}C_4H_6S^*+H^*\rightarrow\alpha,\alpha,\beta\text{-}C_4H_7S^*+*$
4	$\alpha,\beta,\alpha\text{-}C_4H_7S^*+H^*\rightarrow C_4H_8S^*+*$	$\alpha,\beta,\beta\text{-}C_4H_7S^*+H^*\rightarrow C_4H_8S^*+*$	$\alpha,\alpha,\beta\text{-}C_4H_7S^*+H^*\rightarrow C_4H_8S^*+*$
5	$C_4H_8S^*+H^*\rightarrow C_4H_9S^*+*$		
6	$C_4H_9S^*+H^*\rightarrow C_4H_{10}^*+S^*$		
Step	**Mechanism D**	**Mechanism E**	**Mechanism F**
1	$C_4H_4S^*+H^*\rightarrow\beta\text{-}C_4H_5S^*+*$		$C_4H_4S^*+H^*\rightarrow C_4H_5S^*+*$
2	$\beta\text{-}C_4H_5S^*+H^*\rightarrow\beta,\alpha\text{-}C_4H_6S^*+*$		$C_4H_5S^*+H^*\rightarrow C_4H_6^*+S^*$
3	$\beta,\alpha\text{-}C_4H_6S^*+H^*\rightarrow\beta,\alpha,\beta\text{-}C_4H_7S^*+*$	$\beta,\alpha\text{-}C_4H_6S^*+H^*\rightarrow\beta,\alpha,\alpha\text{-}C_4H_7S^*+*$	
4	$\beta,\alpha,\beta\text{-}C_4H_7S^*+H^*\rightarrow C_4H_8S^*+*$	$\beta,\alpha,\alpha\text{-}C_4H_7S^*+H^*\rightarrow C_4H_8S^*+*$	
5	$C_4H_8S^*\ H^*\rightarrow C_4H_9S^*+*$		
6	$C_4H_9S^*+\ H^*\rightarrow C_4H_{10}^*+S^*$		

α, β represents hydrogenation of α-C or β-C

Table 4

Activation energies (*Ea*) and reaction energies (*ΔE*) of elementary reactions on Pd(111) surface

Intermediate	Reaction	*Ea*/(kJ·mol^{-1})	*ΔE*/(kJ·mol^{-1})
TS1	$C_4H_4S^*+H^*\rightarrow\alpha\text{-}C_4H_5S^*+^*$	41.6	-54.6
TS2	$C_4H_4S^*+H^*\rightarrow\beta\text{-}C_4H_5S^*+^*$	85.6	-50.7
TS3	$\alpha\text{-}C_4H_5S^*+H^*\rightarrow\alpha,\beta\text{-}C_4H_6S^*+^*$	142.1	-22.9
TS4	$\alpha\text{-}C_4H_5S^*+H^*\rightarrow\alpha,\alpha\text{-}C_4H_6S^*+^*$	185.6	21.3
TS5	$\alpha,\beta\text{-}C_4H_6S^*+H^*\rightarrow\alpha,\beta,\alpha\text{-}C_4H_7S^*+$	124.2	85.3
TS6	$\alpha,\beta\text{-}C_4H_6S^*+H^*\rightarrow\alpha,\beta,\beta\text{-}C_4H_7S^*+$	110.1	-36.6
TS7	$\alpha,\beta,\beta\text{-}C_4H_7S^*+H^*\rightarrow C_4H_8S^*+^*$	229.9	11.3
TS8	$C_4H_8S^*+H^*\rightarrow C_4H_9S^*+^*$	198.8	-37.8
TS9	$C_4H_9S^*+H^*\rightarrow C_4H_{10}^*+S^*$	169.1	-48.3
TS10	$C_4H_4S^*+H^*\rightarrow C_4H_5S^*+^*$	62.5	-54.6
TS11	$C_4H_5S^*+H^*\rightarrow C_4H_6^*+S^*$	58.6	-90.1